Methane dynamics in the Baltic Sea: investigating concentration, flux and isotopic composition patterns using the coupled physical-biogeochemical model BALTSEM-CH4 v1.0

Erik Gustafsson[1,2], Bo G. Gustafsson[1,2], Martijn Hermans[2,3], Christoph Humborg[2], Christian Stranne[2,4,5]

5   [1]Baltic Nest Institute, Stockholm University, 106 91 Stockholm, Sweden
[2]Baltic Sea Centre, Stockholm University, 106 91 Stockholm, Sweden
[3]Environmental Geochemistry Group, Faculty of Science, University of Helsinki, Helsinki 00560, Finland
[4]Department of Geological Sciences, Stockholm University, 106 91 Stockholm, Sweden
[5]Bolin Centre for Climate Research, Stockholm University, 106 91 Stockholm, Sweden

10   *Correspondence to*: Erik Gustafsson (erik.gustafsson@su.se)

Abstract. Methane (CH$_4$) cycling in the Baltic Sea is studied through model simulations that incorporate the stable isotopes of CH$_4$ (^{12}C-CH$_4$ and ^{13}C-CH$_4$) in a physical-biogeochemical model. A preliminary CH$_4$ budget identifies benthic release as the dominant CH$_4$ source, which is largely balanced by oxidation in the water column and to a smaller degree by outgassing.
The contributions from land loads and net export to the North Sea are of marginal importance. Simulated total CH$_4$ emissions from the Baltic Sea correspond to an average 0.04 g CH$_4$ m^{-2} y^{-1}, which can be compared to the calibrated sediment source of 0.3 g CH$_4$ m^{-2} y^{-1}. A major uncertainty is that spatial and temporal variations of the sediment source are not well known. Further, the coarse spatial resolution prevents the model to resolve shallow-water near-shore areas for which measurements indicate occurrences of considerably higher CH$_4$ concentrations and emissions compared to the open Baltic Sea. Modeling of stable CH$_4$ isotopes can help to constrain process rates; to our knowledge this is the first time that CH$_4$ isotopes have been included in a physical-biogeochemical model. A large-scale approach is used in this study, but the parametrizations and parameters presented here could also be implemented in models of near-shore areas where CH$_4$ concentrations and fluxes are typically substantially larger and more variable. Currently, it is not known how important local shallow-water CH$_4$ hotspots are compared to the open water outgassing in the Baltic Sea.
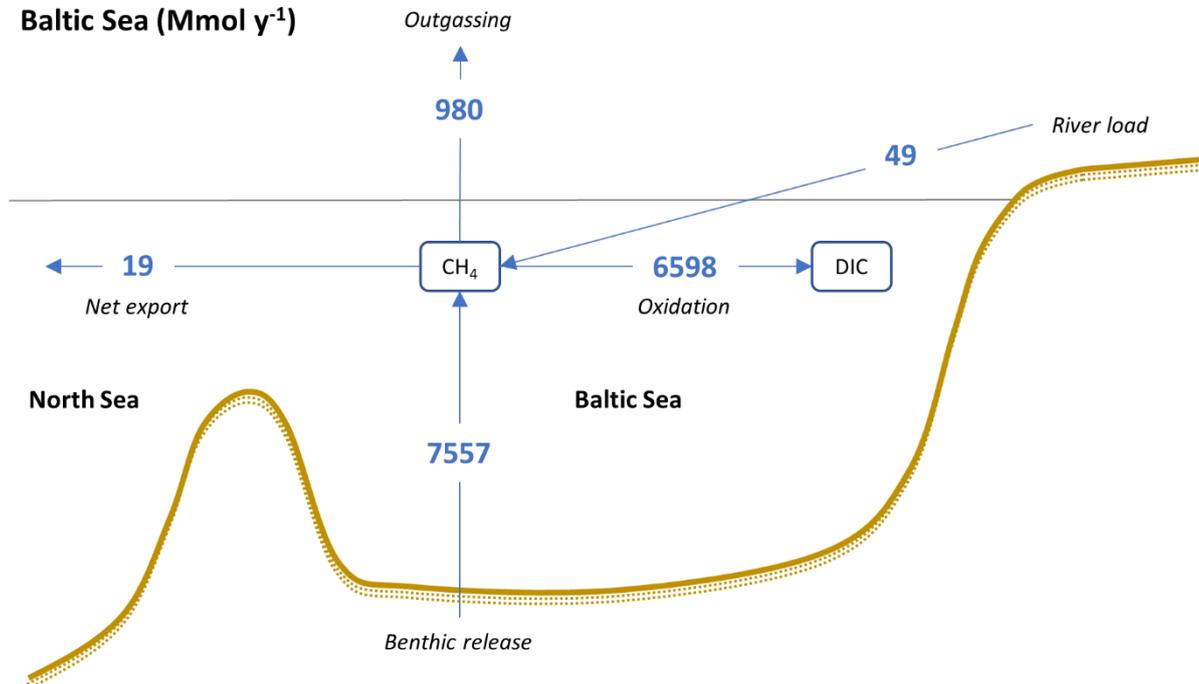
1 Introduction

Methane is the second-most important greenhouse gas after carbon dioxide (CO_2), contributing up to 20% of the total radiative

30 forcing (Etminan et al., 2016). Using top-down approaches (atmospheric observations and inverse modeling), the present-day global CH_4 emissions have been estimated to be 576 Tg CH_4 y^{-1}, whereas bottom-up approaches (process-based modeling of land surface emissions and data on anthropogenic emissions) yield a total of 737 Tg CH_4 y^{-1} (Saunois et al., 2020). The causes of the discrepancy between the two methods are not well known, but is believed to mainly reflect uncertainties in estimates of natural emissions – in particular from wetlands, lakes, and running waters (Saunois et al., 2020). The global mean atmospheric

35 CH_4 level has increased by about 1000 ppb over the last two centuries (Ferretti et al., 2005). Projections of future development ranges from a gradual decrease to a massive increase depending on the development of anthropogenic emissions (Saunois et al., 2020).

The isotopic composition of atmospheric CH_4 ($\delta^{13}C_{CH4a}$) varies seasonally and over longer time-scales (Ferretti et al., 2005; Lan et al., 2021). Long-term trends of $\delta^{13}C_{CH4a}$ depend on the relative contributions from three main sources: biogenic (-110‰

40 to -50‰; e.g., wetlands -60‰), fossil (-40‰), and pyrogenic/biomass burning (-25‰ or -12‰; depending on pathways of carbon fixation in plants). Over the 20th century, a long-term increase of $\delta^{13}C_{CH4a}$ from -49‰ to -47‰ has occurred (Ferretti et al., 2005). However, a recent increase of the atmospheric CH_4 level has been accompanied by a decrease in $\delta^{13}C_{CH4a}$, for reasons that are not fully understood (Lan et al., 2021). The observed $\delta^{13}C_{CH4a}$ development can help to constrain different CH_4 sources and thus reduce their uncertainties.

45 It has been estimated that approximately half of the total CH_4 emissions come from aquatic ecosystem sources, dominated by inland water ecosystems (Rosentreter et al., 2021). The total oceanic CH_4 emissions, including diffusive and bubble-driven ebullitive fluxes, constitute a relatively small fraction amounting to ~6–12 Tg CH_4 y^{-1} (Weber et al., 2019). Methane formation in sediments can be substantial, but aerobic and anaerobic oxidation processes efficiently remove CH_4 both in the pore water and water column when oxidants (e.g., oxygen and sulfate), as well as, methanotrophic bacteria (Broman et al., 2020) are

50 present. For that reason, near-shore areas (0–50 m water depth), shallow enough to allow CH_4 to escape to the atmosphere before being oxidized, dominate the oceanic emissions despite representing a comparatively minor area (Weber et al., 2019). In shallow, organic-rich sediments, CH_4 emissions will increase in response to ocean warming due to increased biogenic CH_4 production and decreased CH_4 solubility, both of which promote seafloor ebullition (Borges et al., 2016). This notion was confirmed in a recent field study where exceptionally high CH_4 emissions were reported from the coastal Baltic Sea at the end

55 of a summer heat wave (~250 µmol m^{-2} day^{-1}, Humborg et al., 2019).

In the Baltic Sea, there are strong gradients in CH_4 concentrations both from near-shore areas to open Baltic Sea surface waters (e.g., Humborg et al., 2019) and from surface to deep water (e.g., Schmale et al., 2010; Jakobs et al., 2013). Substantial parts of Baltic Sea deep waters are stagnant over extended periods in time, which in combination with high loads of organic material cause episodic anoxia (e.g., Carstensen et al., 2014). During stagnant anoxic periods, CH_4 accumulates and reaches

60 concentrations ranging from 1000 to 3000 nM (Jakobs et al., 2013; 2014). This CH_4 is, however, largely consumed by aerobic

oxidation processes (MOX) when mixed into the redox zone at intermediate depths (Jakobs et al., 2013). Peak oxidation rates have consequently been observed in the redox zone where deep water enriched in CH_4 is mixed with oxic water (Jakobs et al., 2013). Due to the special characteristics of deep water areas isolated from the atmosphere, and with transitions between oxic and anoxic conditions, the Baltic Sea is a unique and suitable system for studying key processes in CH_4 cycling, in particular

65 for investigating different oxidation pathways.

Surface water CH_4 concentrations in the open Baltic Sea are typically about 3.5–5 nM – only slightly oversaturated compared to the atmosphere (Gülzow et al., 2013). In contrast, in shallow near-shore areas, observations indicate a very different situation, with CH_4 concentrations ranging from 10 to 500 nM (Humborg et al., 2019; Myllykangas et al., 2020; Lundevall-Zara et al., 2021; Roth et al., 2022) with large temporal and spatial variations on small scales (e.g., Roth et al., 2022). Methane

70 emissions to the atmosphere depend on the degree of oversaturation in the surface water, but also on wind speed and temperature (e.g., Wanninkhof, 2014). Estimated CH_4 emissions from different near-shore sites in the Baltic Sea display a large range due to substantial variations in the parameters that control gas transfer across the air-sea interface (Humborg et al., 2019; Lundevall-Zara et al., 2021; Asplund et al., 2022; Roth et al., 2022; 2023). Short-term and small-scale variations cause considerable challenges for empirical estimates of fluxes over larger scales and longer periods in time.

75 Different processes in the CH_4 cycling do, however, produce certain "fingerprints" on the isotopic composition, similar to how the relative contributions of different atmospheric CH_4 sources determine long-term trends of $\delta^{13}C_{CH4a}$ (Lan et al., 2021). This can be helpful when assessing process rates. Observations in the Baltic Sea show a pronounced ^{13}C-CH_4 enrichment in the redox zone (Schmale et al., 2012; 2016; Jakobs et al., 2013; 2014; Gülzow et al., 2014), which is the result of a preferential oxidation of the lighter isotope. Similarly, CH_4 emissions to the atmosphere can produce a ^{13}C-CH_4 enrichment in the surface

80 water because of a preferential outgassing of the lighter isotope (Knox et al., 1992). The isotopic composition of CH_4 produced in sediments depends on the processes involved, i.e., CO_2 reduction or acetate fermentation (Reeburgh, 2007; see also Sect. 2.3.5), but can then be modified by oxidation processes in the pore water (Chuang et al., 2019).

Models can be useful for identifying limiting processes and constraining budgets even though not all rates are well known, through sensitivity experiments on process rates and parameterizations, as well as on the influence of changes in forcing of the

85 system. Methane cycling has previously been investigated in lake modeling studies (e.g., Lopes et al., 2011; Greene et al., 2014; Bayer et al., 2019). Furthermore, CH_4 emissions from the Arctic shelf have been addressed by means of model simulations (Wåhlström and Meier, 2014; Malakhova and Golubeva, 2022). Wåhlström and Meier (2014) examined the sensitivity of CH_4 emissions depending on riverine CH_4 concentration, release rate from the sediments, and oxidation rate in the water column. None of the abovementioned models, however, included stable CH_4 isotopes. In the present study, CH_4

90 cycling and dynamics in the Baltic Sea are introduced into the coupled physical-biogeochemical Baltic Sea long-term and large-scale eutrophication model (BALTSEM), by expanding with state variables for both ^{12}C-CH_4 and ^{13}C-CH_4 concentrations (see Sect. 2.2). BALTSEM has previously been used in a similar approach where stable isotopes of dissolved inorganic carbon as well as dissolved and particulate organic carbon were included in the model in order to investigate constraints on process rates (Gustafsson et al., 2015).

95 Benthic CH$_4$ release and the isotopic composition of CH$_4$ produced in the sediments are not well known except for a few specific sites where *in-situ* measurements have been acquired. This means that the model is, at this point, somewhat poorly constrained. The main objective of this study is to use the model in concert with observed water column CH$_4$ concentrations and isotopic compositions to 1. identify and roughly quantify key CH$_4$ fluxes, 2. set up a preliminary CH$_4$ budget on a Baltic Sea scale, and 3. perform sensitivity experiments on CH$_4$ concentration and isotopic composition depending on transport and

100 transformation processes.

The motivation for implementing the CH$_4$ modeling on a Baltic Sea scale – with considerable spatial differences in terms of e.g., water and sediment properties as well as production, respiration, and sedimentation patterns – was utilizing the application of an already well-established model. BALTSEM has been described and validated in many publications, and it has been demonstrated that both physical (e.g., salinity, temperature, vertical mixing, lateral exchange, air-sea exchange) and

105 biogeochemical (e.g., carbon and nutrient cycling and oxygen production/consumption) processes are largely described satisfactory (Gustafsson et al., 2012; 2017; Savchuk et al., 2012).

2 Material and methods

2.1 Area description

The Baltic Sea is a semi-enclosed brackish sea, connected to the North Sea via the shallow and narrow Danish straits. The

110 system is characterized by a pronounced horizontal salinity gradient – going from the almost oceanic entrance area to the low-saline northernmost sub-basin – as well as a permanent salt dominated stratification, restricted water exchange with the North Sea, and long residence times (e.g., Stigebrandt and Gustafsson, 2003). As a result of strong stratification and long residence times, the central Baltic Sea is naturally susceptible to deep water de-oxygenation. Massively increased nitrogen (N) and phosphorus (P) loads from the early 1950s to the mid-1980s has caused a large expansion of de-oxygenated deep water areas

115 (e.g., Gustafsson et al., 2012). The loads have declined substantially from the peak values in the 1980's (e.g., Kuliński et al., 2022), although oxygen conditions have not yet improved in the central Baltic Sea (Hansson and Viktorsson, 2021).

2.2 The model

BALTSEM is a process-based coupled physical-biogeochemical 1D-model that divides the Baltic Sea into thirteen sub-basins that are horizontally homogenous, but with a high (~1 m) vertical resolution (Fig. S1). The standard model includes pelagic

120 state variables for salinity, temperature, oxygen (O$_2$), hydrogen sulfide, total alkalinity, dissolved inorganic carbon, nitrate, ammonium, phosphate, dissolved silica, labile and refractory fractions of dissolved organic carbon (C), nitrogen (N), and phosphorus (P), particulate organic C, N, P, and Si (biogenic Si), three functional groups of phytoplankton (representing diatoms, 'summer species', and diazotrophic cyanobacteria), and one bulk state variable for heterotrophs (representing all processes that mineralize organic matter). All pelagic state variables are subject to transport processes (vertical mixing and

125 horizontal advection between sub-basins) as well as various biological and chemical transformation processes. BALTSEM

further includes depth dependent sediment pools of C, N, P, and Si that are subject to mineralization, shelf-to-basin transport, and burial.

In this study, a new expanded version of the model, BALTSEM-CH$_4$ v1.0, with state variables for both ^{12}C-CH$_4$ and ^{13}C-CH$_4$ is presented for the first time. BALTSEM-CH$_4$ v1.0 is an expansion of BALTSEM v9.5 (Gustafsson et al., 2023). Source code,

130 model forcing, boundary conditions, and initial profiles are archived on Zenodo at https://doi.org/10.5281/zenodo.10037197. Figure 1 illustrates processes involved in CH$_4$ cycling that are included in the model. The model (prior to the inclusion of CH$_4$) has been described and validated in detail in earlier publications (see Gustafsson et al. (2017) and references therein); this will not be repeated here. A list of all state variables (Table A1) is included in Appendix A. Further, the model forcing is briefly described in Appendix B.

135 This study focuses on the modeling of stable CH$_4$ isotopes: The CH$_4$ sources (i.e., land load and sediment release), boundary conditions (i.e., atmospheric CH$_4$ and CH$_4$ at the model boundary), transport and transformation processes (i.e., CH$_4$ oxidation and air-sea exchange), as well as the isotopic fingerprints associated with these processes are described in Sect. 2.3. An initial model run over the period 1970-2000 started with initial profiles for the different state variables based on observations when possible or else calibrated values. The initial model run was then used as a spin-up for a series of model runs covering the

140 period 2001-2020 that are performed to examine the sensitivity of e.g., CH$_4$ concentration and isotopic composition depending on process parameterizations (Sect. 4.1).
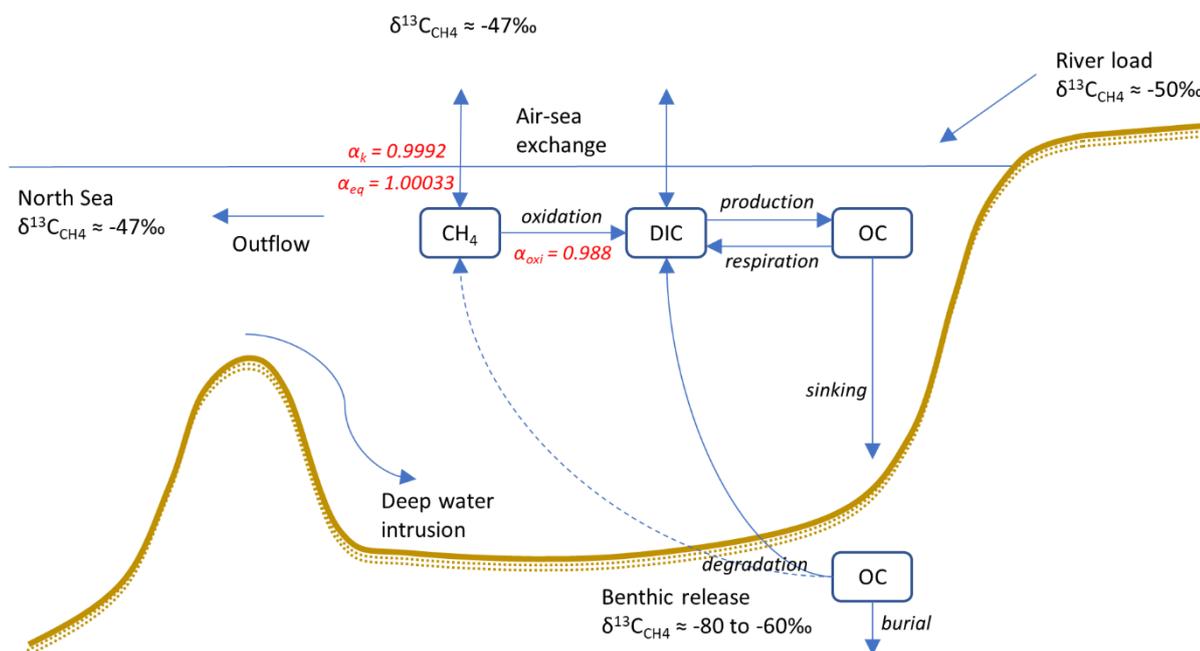
Figure 1: Conceptual sketch illustrating the processes involved in CH₄ cycling, including $\delta^{13}C_{CH4}$ values of end-members as well as
145 **α values of transformation processes (see Sect. 2.3). The benthic release (dashed arrow) is not explicitly modeled, instead a preset calibrated value is used (see Sect. 2.3.5).**

2.3 Methane modeling

2.3.1 Isotopic fractionation

150 Isotope values of CH₄ are expressed in $\delta^{13}C$ units (‰) relative to the Vienna Peedee Belemnite (VPDB) standard (Hoffmann and Rasmussen, 2022):

$$\delta^{13}C = \left(\frac{R_{sample}}{R_{std}} - 1\right) * 1000, \tag{1}$$

155 Here, R_{sample} and R_{std} represent the $^{13}C/^{12}C$ ratios of a sample and the PDB standard, respectively.

Isotopic fractionation α during different processes (e.g., oxidation, air-sea exchange) in the CH₄ cycling can be expressed as:

$$\alpha = \frac{R_A}{R_B}, \tag{2}$$

160 Here, R_A and R_B represent $^{13}C/^{12}C$ ratios of compounds A and B.

Fractionation can also be expressed in $\delta^{13}C$ units using Eq. 1 and 2:

$$\alpha = \left(\frac{\delta_A}{1000} + 1\right) / \left(\frac{\delta_B}{1000} + 1\right), \tag{3}$$

165 Alternatively, fractionation is often expressed as ε values (Zeebe and Wolf-Gladrow, 2001):

$$\varepsilon = \delta_A - \delta_B \approx (\alpha - 1) * 1000, \tag{4}$$

In the model description below, both α and ε values are used to describe fractionation during different processes.

170 ### 2.3.2 Air-sea exchange

The CH₄ flux (F_{CH4}) between water and air is calculated according to:

$$F_{CH4} = k\left(CH_{4eq} - CH_{4w}\right), \tag{5a}$$

$$CH_{4eq} = K_0 pCH_{4a},\tag{5b}$$

175

where k (m s^{-1}) is the transfer velocity, CH_{4eq} the equilibrium concentration with the atmosphere, K_0 (nM atm^{-1}) the CH$_4$ solubility, pCH_{4a} (atm) the partial pressure of CH$_4$ in air, and CH_{4w} (nM) the CH$_4$ concentration in surface water.

The solubility is calculated as a dimensionless Bunsen coefficient (β) according to Wiesenburg and Guinasso (1979):

180 $$\ln\beta = A_1 + A_2(100/TK) + A_3\ln(TK/100) + S(B_1 + B_2(TK/100) + B_3(TK/100)^2),\tag{6}$$

Here, A_1, A_2, A_3, B_1, B_2, and B$_3$ are constants and TK is temperature (K).

β is then converted to K_0 (nM atm^{-1}) according to:

185 $$K_0 = \frac{P_S\beta}{RT_S} * 10^6,\tag{7}$$

where P_S = 101325 Pa atm^{-1} represents a unit conversion from Pa to atm, R = 8.314 m^3 Pa K^{-1} mol^{-1} is the molar gas constant, and T_S = 273.15 K is the standard temperature.

The transfer velocity k is calculated according to Wanninkhof (2014) and converted from cm hour^{-1} to m s^{-1}:

190

$$k = 0.251 U_{10}^2\sqrt{\frac{660}{Sc}} * \frac{0.01}{3600},\tag{8}$$

Here, U_{10} (m s^{-1}) is the wind speed at 10 m height and Sc is the Schmidt number for CH$_4$ (Wanninkhof, 2014):

195 $$Sc = A + BT + CT^2 + DT^3 + ET^4,\tag{9}$$

Here, A, B, C, D, and E are constants and T is temperature (°C).

The atmospheric CH$_4$ level has increased from around 800 ppb to almost 1900 ppb over the last two centuries (see Fig. S2). In the different model runs, the atmospheric CH$_4$ levels according to the RCP 4.5 scenario were used (Fig. S2). The mixing ratio

200 is expressed as mole fraction of dry air (ppb) and thus identical to the CH$_4$ partial pressure, pCH$_{4a}$ (natm).

Fractionation during gas transfer and dissolution

The fractionation of a gas during transfer between air and water depends on two fractionation processes – gas dissolution and molecular gas transfer. The fractionation α_{eq} during dissolution of CH$_4$ in water is defined as (Knox et al., 1992):

205

$$\alpha_{eq} = \frac{R_{CH4eq(d)}}{R_{CH4eq(g)}}, \tag{10}$$

Here, $R_{CH4eq(d)}$ and $R_{CH4eq(g)}$ represent the ratios of the heavy and light CH_4 isotopes between the equilibrium concentrations of CH_4 in dissolved (d) and gas phase (g), respectively. Experiments by Fuex (1980) indicate that the heavy CH_4 isotope is more

210   soluble than the lighter isotope (although the lighter isotope initially dissolves faster), with a fractionation during dissolution amounting to approximately $\alpha_{eq} = 1.00033$.

A difference in the molecular transfer rates of heavy and light CH_4 isotopes, result in further fractionation defined as (Knox et al., 1992):

215   $$\alpha_k = \frac{k_{13CH4}}{k_{12CH4}}, \tag{11}$$

Here, k_{13CH4} and k_{12CH4} represent the transfer rates of the heavy and light isotope, respectively. Experiments by Knox et al. (1992) indicate a preferential exchange of the light isotope, with a fractionation during gas transfer of approximately $\alpha_k = 0.9992$. Measurements from stagnant wooded swamps point to a reduced gas exchange but also a considerably more

220   pronounced kinetic fractionation in waters with insoluble organic surface films (Happell et al., 1995). Surface films are, however, not taken into account in BALTSEM-CH_4 v1.0.

The ^{13}C-CH_4 flux between water and air, F_{13CH4}, is calculated based on Holmes et al. (2000):

$$F_{13CH4} = k\alpha_k\left(K_0 pCH_{4a}R_{atm}\alpha_{eq} - \left[^{13}CH_{4w}\right]\right), \tag{12}$$

225

Here, R_{atm} is the ^{13}C/^{12}C ratio of atmospheric CH_4, and $[^{13}CH_{4w}]$ is the surface water concentration of ^{13}C-CH_4.

In the model runs, the atmospheric $\delta^{13}C_{CH4}$ is set to a constant -47‰.

2.3.3 River loads

Measurements in Swedish low-order streams (Strahler stream order 1-4) indicate a median CH_4 concentration of approximately

230   6.7 µg C L^{-1} – corresponding to 560 nM – but with substantial variations between individual streams (Wallin et al., 2018). As opposed to CO_2 concentrations that generally declined with increasing stream order, there was no such clear relation between stream order and median CH_4 concentration, although the lowest median concentration (3.6 µg C L^{-1}, corresponding to 300 nM) was reported for the largest streams (Wallin et al., 2018).

CH_4 produced in freshwater sediments and wetlands is presumably mainly resulting from acetate fermentation (see Sect. 2.3.5),

235   with isotope values in a typical range -65‰ to -50‰ (Whiticar et al., 1986; Quay et al., 1988). However, both CH_4 oxidation and outgassing cause a ^{13}C enrichment in the residual CH_4 pool. This means that an increasing isotope value is expected as outgassing and oxidation processes gradually modulate both CH_4 concentrations and isotopic composition in streams and rivers

along their routes towards the sea. Measurements in a subtropical river network in Australia indicate surface water $\delta^{13}C_{CH4}$ values in a range -57‰ to -47‰ (Atkins et al., 2017), i.e., values close to, or lower than the atmospheric $\delta^{13}C_{CH4}$ (see Sect.

240   2.3.2). Similarly, measurements in an urbanized river system in Scotland indicate $\delta^{13}C_{CH4}$ values in a range -60‰ to -47‰ (Gu et al., 2021).

As a fist approximation, it will be assumed that the riverine CH_4 concentration (CH_{4riv}) is 100 nM and that $\delta^{13}C_{CH4}$ = -50‰ in rivers entering the Baltic Sea.

2.3.4 Inflows from the North Sea

245   Methane concentrations in open North Sea surface waters are highly heterogeneous, but generally above the solubility equilibrium with the atmosphere. Observations indicate a range 3 - 30 nM (Bange et al., 1994; Rehder et al., 1998; Osudar et al., 2015). This heterogeneity has been suggested to partly be a result of the westward transport of surface waters originating from the Kattegat and Skagerrak (Rehder et al., 1998). Closer to the coasts where both rivers and coastal sediments can be significant regional sources of CH_4, concentrations are usually considerably higher (Scranton and McShane, 1991; Rehder et

250   al., 1998; Upstill-Goddard et al., 2000; Grunwald et al., 2009; Osudar et al., 2015), but large fractions appear to be removed within estuaries before reaching the open sea (Upstill-Goddard et al., 2000; Grunwald et al., 2009). Measurements from the southern central North Sea indicate concentrations close to (but higher than) the equilibrium (Scranton and McShane, 1991; Bange et al., 1994; Rehder et al., 1998).

As a fist approximation, it will be assumed that the CH_4 concentration is 5 nM and that $\delta^{13}C_{CH4}$ = -47‰ in North Sea water

255   entering the Baltic Sea.

2.3.5 Benthic release

Methanogenesis

There are two primary methanogenic pathways for biologically mediated CH_4 production – CO_2 reduction and acetate fermentation (Reeburgh, 2007):

260

$$CO_2 + 4H_2 \rightarrow CH_4 + 2H_2O, \tag{13}$$
$$CH_3COOH \rightarrow CH_4 + CO_2, \tag{14}$$

CO_2 reduction is dominant in the sulfate depleted zone of marine sediments, whereas acetate fermentation is dominant in

265   freshwater sediments. Both pathways may nevertheless occur in both marine and limnic environments (Whiticar et al., 1986). Methanogenesis in marine environments is assumed to predominantly occur in anoxic sediments, whereas the presence of oxygen and/or sulfate generally prevents large-scale methanogenesis in the water column. In anoxic sediments, sulfate can be used as an oxidant during mineralization of organic matter or consumed by sulfate mediated oxidation of CH_4. The sediment depth of sulfate depletion and the main zone of methanogenesis depend strongly on location and sedimentation rate.

270 Measurements in the Baltic Sea area indicate sulfate depletion depths in a range of centimeters to meters (Jørgensen et al., 1990; Slomp et al., 2013; Myllykangas et al., 2020).

The default sediment source is set to 50 µmol m^{-2} d^{-1}, which is a calibrated value that produces deep water CH_4 observations reasonably well. The impact from the sediment source is further explored in different sensitivity experiments (Sect. 4.1).

275 *Fractionation during methanogenesis*

Isotope values of CH_4 from biogenic sources are typically in a range -110‰ to -60‰ (Whiticar et al., 1986), depending on methanogenic substrate and mechanisms (i.e., CO_2 reduction vs. acetate fermentation). The fractionation during CO_2 reduction is typically $\varepsilon > 95$‰, while the fractionation during acetate fermentation is in a range $\varepsilon \sim 40$-60‰ (Whiticar, 1999).

Measurements from anoxic deep water in the central Baltic Sea show isotope values of -84‰ and -71‰ in the Gotland and

280 Landsort Deeps, respectively (Jakobs et al., 2013). Deep water in the Bornholm basin shows isotope values of approximately -70‰, and deep water in the Arkona basin show isotope values in a range -69‰ to -63‰ (Gülzow et al., 2014). Measurements by Roth et al. (2022) indicate a value of approximately -67‰ for the sediment source in shallow areas with oxic conditions in the water column. Furthermore, measurements by Egger et al. (2017) indicate surface sediment pore water $\delta^{13}C$-CH_4 values of approximately -80‰ in the Landsort Deep (451 mbss), -70‰ in the Bornholm Deep (87 mbss), and -60‰ in the Little Belt

285 (37 mbss).

As a first approximation, the sediment CH_4 source in the model is assumed to have a $\delta^{13}C$-CH_4 value of -80‰ or -60‰ in sediments underlying anoxic or oxic water, respectively. This value will then be adjusted in different sensitivity experiments (Sect. 4.1).

2.3.6 Methane oxidation in the water column

290 *Methane oxidation by oxygen (MOX)*

Aerobic CH_4 consumption by methanotrophic processes consume CH_4 and oxygen while producing CO_2 and water:

$$CH_4 + 2O_2 \rightarrow CO_2 + 2H_2O, \tag{15}$$

295 The oxidation rate, W_{CH4_O2} (nM day^{-1}) is parameterized as Monod functions of both CH_4 (nM) and O_2 (µM) concentrations (Van Bodegom et al., 2001; Greene et al., 2014):

$$W_{CH4\_O2} = v_{WCH4\_O2} \left(\frac{[CH_4]}{h_{CH4}+[CH_4]} \right) \left(\frac{[O_2]}{h_{O2}+[O_2]} \right), \tag{16}$$

300 Here, v_{WCH4_O2} (nM d^{-1}) is the potential maximum aerobic oxidation rate, *[CH4]* (nM) and *[O2]* (µM) are CH_4 and O_2 concentrations, whereas h_{CH4} (nM) and h_{O2} (µM) are "half saturation" concentrations for CH_4 and O_2, respectively.

Aerobic oxidation of CH_4 is also included as an O_2 sink term in the model, consuming 2 mol O_2 for each mol of consumed CH_4 (Eq. 15). Furthermore, both aerobic and anaerobic CH_4 oxidation are included as sources of dissolved inorganic carbon in the model, producing 1 mol of DIC for each mol of consumed CH_4 (Eq. 15 and 17, respectively).

305 Observations from the Gotland and Landsort deeps in the Baltic Proper indicate oxidation rates in a range 0.1-4 nM d^{-1} depending on location and season (Schmale et al., 2012; 2016; Jakobs et al., 2014). The parameters in Eq. 16 are set to default values of v_{WCH4_O2} = 8 nM d^{-1}, h_{CH4} = 60 nM, and h_{O2} = 100 µM. These are calibrated values that produce CH_4 concentrations and oxidation rates that fairly well reproduce observations (see Sect. 3.1). In Sect. 4.1, the influence of modified values of v_{WCH4_O2}, h_{CH4}, and h_{O2} will be addressed in different sensitivity experiments.

310

Anaerobic oxidation of CH_4 by sulfate (AOM)

AOM is typically assumed to be mediated by sulfate, although other oxidants such as nitrate/nitrite and also iron and manganese oxides could be used as well (Myllykangas et al., 2020). The stoichiometry for sulfate mediated AOM can be written (Hoehler et al., 1994):

315

$$CH_4 + SO_4^{2-} \rightarrow HS^- + HCO_3^- + H_2O, \tag{17}$$
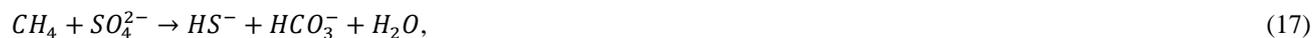
The ratios of sulfate and chlorine concentrations in the Baltic Sea are close to the oceanic ratio (Kremling, 1972), which means that the sulfate concentration $[SO_4^{2-}]$ in the Baltic Sea can be approximated as

320

$$[SO_4^{2-}] \approx [SO_4^{2-}]_{oc} \frac{S}{35}, \tag{18}$$

Here, S is the salinity and $[SO_4^{2-}]_{oc}$ = 0.0282 mol kg^{-1} is the sulfate concentration in sea water (S = 35) (Dickson et al., 2007). Thus, sulfate concentrations in the Baltic Sea are orders of magnitude higher than CH_4 concentrations. For that reason, CH_4

325 oxidation by sulfate, W_{CH4_SO4} (nM day^{-1}) is parameterized as a function of CH_4, whereas the sulfate concentration is assumed not to be limiting in the water column:

$$W_{CH4\_SO4} = v_{WCH4\_SO4} \left(\frac{[CH_4]}{h_{CH4} + [CH_4]} \right), \tag{19}$$

330 Since sulfate is assumed not to be limiting, other potential oxidants during AOM are not accounted for in the model. Observations from the anoxic deep waters of the Gotland and Landsort deeps in the Baltic Proper indicate oxidation rates < 0.1 nM d^{-1} (Jakobs et al., 2014). The maximum anaerobic oxidation rate is set to a default value of v_{WCH4_SO4} = 0.1 (nM d^{-1}).

Fractionation during CH_4 oxidation

335   There is a preferential oxidation of ^{12}C-CH$_4$ compared to the heavier ^{13}C-CH$_4$, causing a fractionation during the process. The oxidation of ^{13}C-CH$_4$ is thus computed according to:

$$W_{13CH4\_O2} = \alpha_{oxi} R_{CH4} W_{CH4\_O2},$$ (20)

340   Here, α_{oxi} is the fractionation during CH$_4$ oxidation, R_{CH4} is the ^{13}C/^{12}C ratio of CH$_4$, and W_{CH4_O2} is the CH$_4$ oxidation rate (Eq. 16). By use of Eq. 16, Eq. 20 can be rewritten as:

$$W_{CH4\_O2} \approx \alpha_{oxi} v_{WCH4\_O2} \left(\frac{[^{13}CH_4]}{h_{CH4} + [CH_4]} \right) \left(\frac{[O_2]}{h_{O2} + [O_2]} \right),$$ (21)

345   Observations of fractionation during CH$_4$ oxidation indicate fractionation values in a range $\varepsilon \sim$ 4-30‰ (Whiticar, 1999). Based on observations from the central Baltic Sea by Jakobs et al. (2013), the default fractionation is set to 12‰, which corresponds to α_{oxi} = 0.988 in Eq. 20. The influence of fractionation during CH$_4$ oxidation is addressed by sensitivity experiments in Sect. 4.1.

3 Results

350   In this section, simulated CH$_4$ concentrations, isotopic compositions, and aerobic and anaerobic oxidation rates are presented for a 'standard' model run (Sect. 3.1). Simulated large-scale fluxes and a preliminary CH$_4$ budget are presented in Sect. 3.2.

3.1 Standard model run

The standard model run was performed over the period 2001-2020 after spin-up (see Sect. 2.2) with parameters as indicated in Table 1. These parameters are mostly calibrated values, where the intension was to reasonably well reproduce existing
355   observations from the Gotland Sea. This simulation will then be used as a basis for the sensitivity experiments presented in Sect. 4.1. Simulated contour plots and time series for the period 2001-2020 are presented in Fig. 2-3. Furthermore, monthly mean profiles for years 2014 and 2015 are presented in Fig. 4-5 in order to illustrate seasonal dynamics in surface waters as well as the impact of a major deep water inflow.

360   Table 1. Standard model settings. The values are own estimates/calibrated values (see Sect. 2.3) except where noted.

Parameter	Notation	Value	Unit
Potential maximum oxidation rate (MOX)	v_{WCH4_O2}	8	nM d^{-1}
Potential maximum oxidation rate (AOM)	v_{WCH4_SO4}	0.1	nM d^{-1}
Half saturation value, CH$_4$ oxidation	h_{CH4}	60	nM

Half saturation value, CH$_4$ oxidation	h_{O2}	100	µM
Fractionation, CH$_4$ oxidation	α_{oxi}	0.988[1]	-
Sediment source, CH$_4$ flux	r_{SED}	50	µmol m^{-2} d^{-1}
Sediment source, δ^{13}C-CH$_4$, anoxic water	$\delta^{13}C\text{-}CH_{4sed}$	-80	‰
Sediment source, δ^{13}C-CH$_4$, oxic water	$\delta^{13}C\text{-}CH_{4sed}$	-60	‰
Riverine CH$_4$	CH_{4riv}	100	nM
Riverine δ^{13}C-CH$_4$	$\delta^{13}C\text{-}CH_{4riv}$	-50	‰
North Sea CH$_4$	CH_{4NS}	5	nM
North Sea δ^{13}C-CH$_4$	$\delta^{13}C\text{-}CH_{4NS}$	-47	‰

1. Jakobs et al. (2013)

Figure 2 illustrates the characteristic dynamics of the permanently salinity stratified Gotland Sea. The top of the halocline, which is typically located at around 60 m depth, isolates deeper waters from the atmosphere which means that O$_2$ can only be
365 supplied via deep water inflows of oxic and comparatively high-saline water and through vertical turbulent diffusion. Stagnation periods with little or no advective O$_2$ supply to the deep may last for years, and since O$_2$ consumption by degradation processes exceeds the turbulent diffusive flux eventually conditions anoxic prevails. Stagnation periods are also characterized by CH$_4$ accumulation because of a low anaerobic oxidation rate, and the δ^{13}C-CH$_4$ in anoxic water is also close to the sediment source because of the marginal influence of anaerobic oxidation processes in the water column. Inflows of new deep water
370 lead to an uplift of the water column above the intrusion depth, which is clearly seen in the simulated O$_2$ and CH$_4$ profiles in February to June of 2015 (Fig. 5, upper panel). Inflows furthermore cause a sharp decline in deep water CH$_4$ concentration (Fig. 2-3), primarily due to water exchange, but additionally because of high aerobic oxidation rates during periods when O$_2$ and CH$_4$ co-occur in the deep water until O$_2$ is again depleted (Fig. 5).
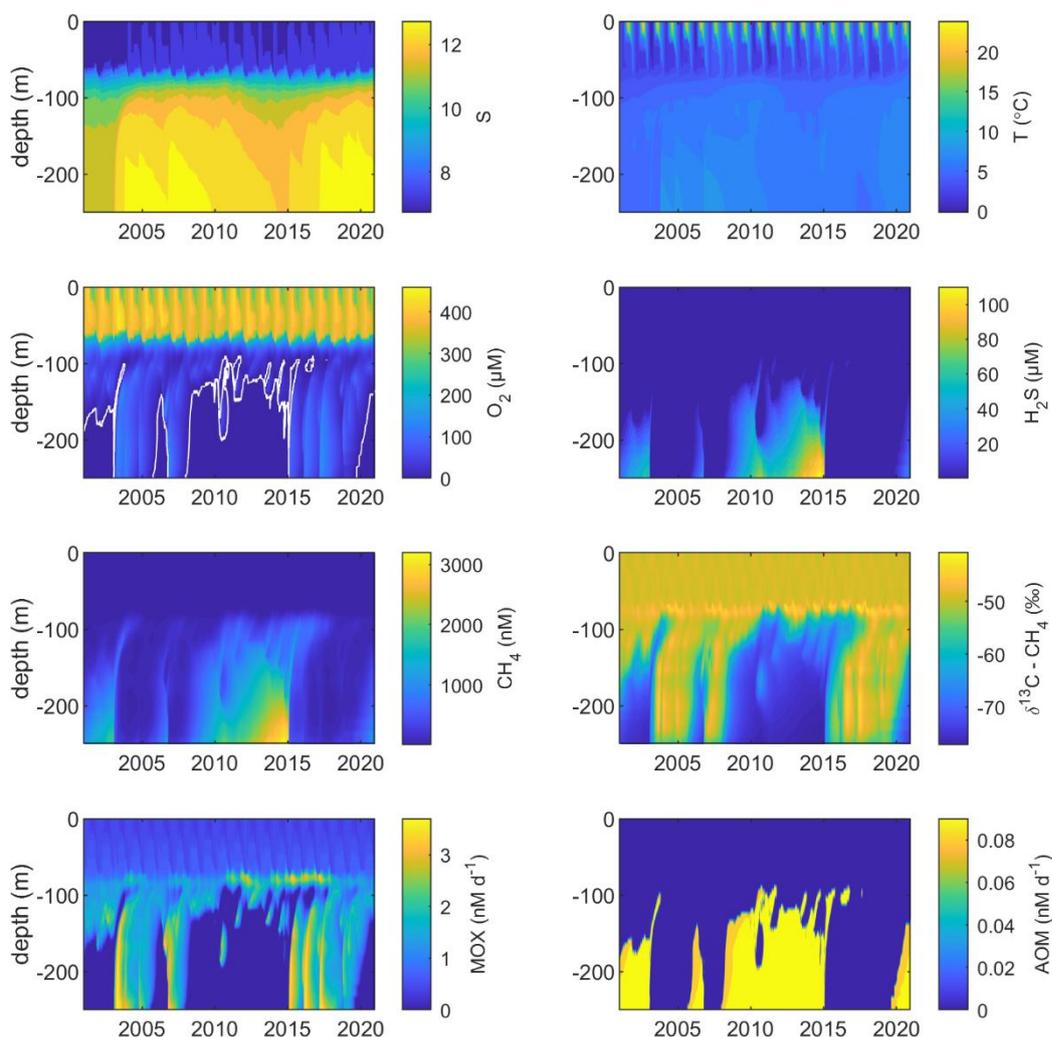
375

Figure 2: Model output from the standard model run, showing simulated S, T (°C), O_2 (µM), H_2S (µM), CH_4 (nM), $\delta^{13}C$-CH_4 (‰), MOX (nM d^{-1}), and AOM (nM d^{-1}) in the Gotland Sea sub-basin (cf. Fig. S1) over the period 2001-2020. The white line in the O_2 plot indicates the upper limit for anoxic deep water.
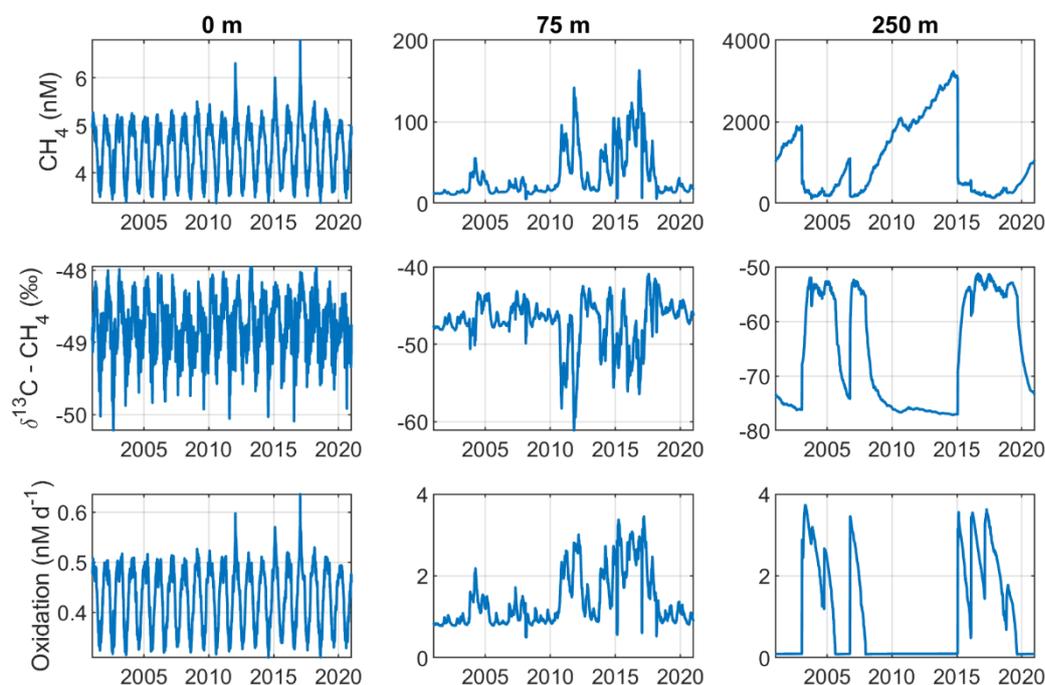
Figure 3: Model output from the standard model run, showing simulated surface (0 m; left-hand panels), intermediate (75 m; middle panels), and deep water (250 m; right-hand panels) development of CH₄ (nM), CH₄ oxidation (MOX + AOM; nM d⁻¹), and δ¹³C-CH₄ (‰) in the Gotland Sea sub-basin (cf. Fig. S1) over the period 2001-2020.

In surface waters above the top of the halocline, seasonal changes in temperature and thermal stratification largely influence other parameters (Fig. 4-5; see also Fig. S3-S4, supporting information). The increasing surface water temperature in spring and summer leads to decreasing O_2 and CH_4 solubility which in addition affects aerobic oxidation rates that depend on O_2 and CH_4 concentrations (Fig. S3-S4, supporting information; see also Eq. 16). The $\delta^{13}C\text{-}CH_4$ in water above the top of the halocline is thus strongly influenced by the seasonality of temperature stratification, although the amplitude is significantly smaller than the variations at depth where $\delta^{13}C\text{-}CH_4$ mainly depend on transitions between oxic and anoxic conditions.
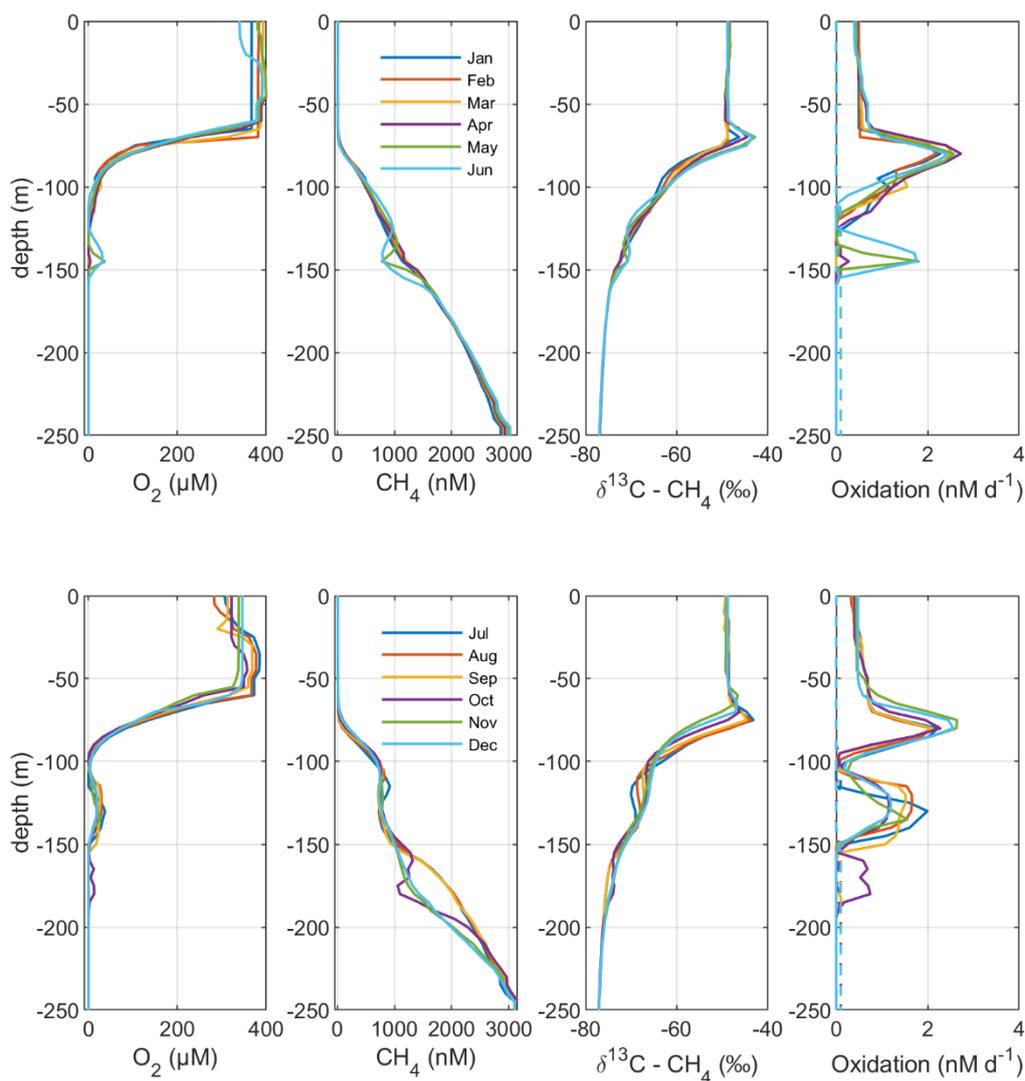
Figure 4: Model output from the standard model run, showing simulated monthly mean profiles of CH₄ (nM), δ¹³C-CH₄ (‰), and oxidation rates (nM d⁻¹; MOX – full lines, AOM – dashed lines) in the Gotland Sea sub-basin (cf. Fig. S1) year 2014. The upper panels illustrate monthly mean profiles from January to June; the lower panels illustrate monthly mean profiles from July to December.
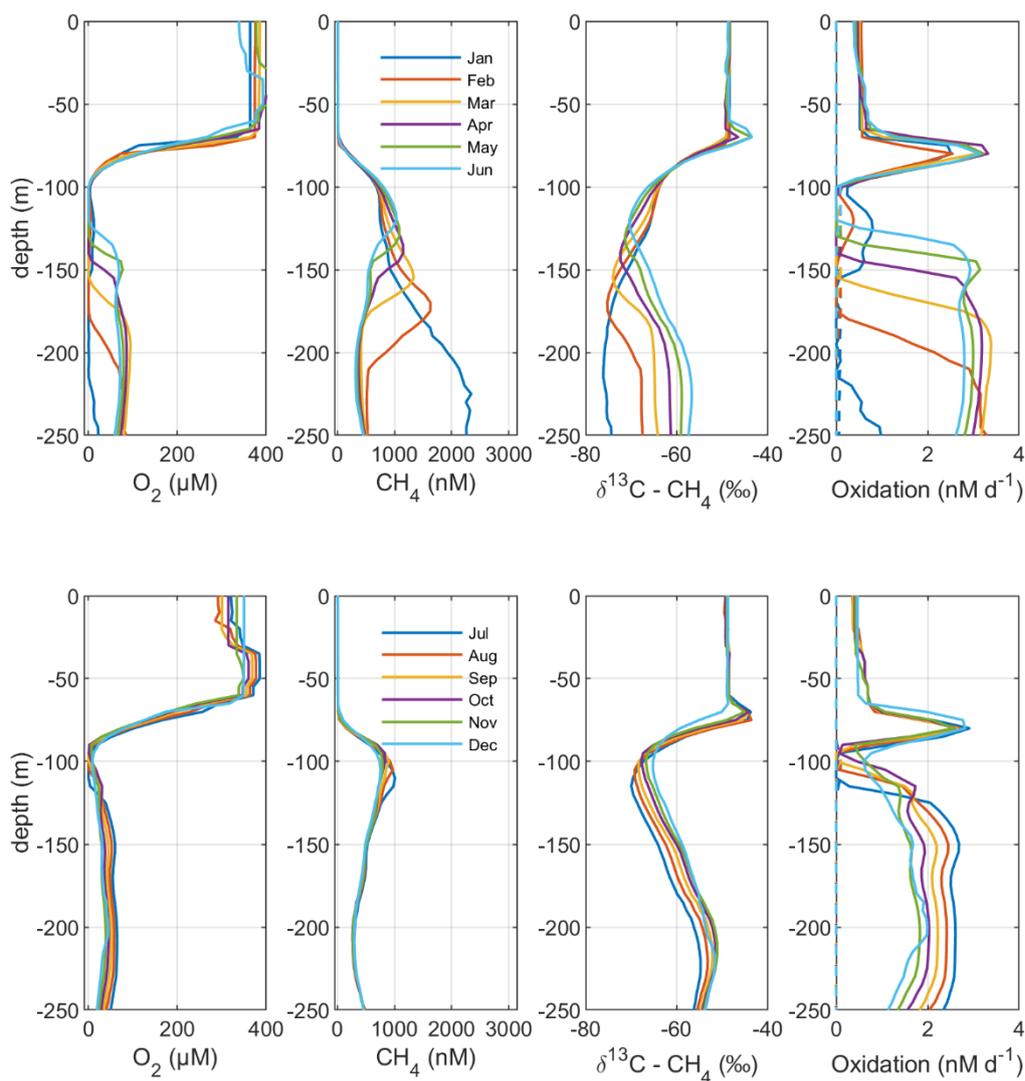
Figure 5: Model output from the standard model run, showing simulated monthly mean profiles of CH₄ (nM), δ¹³C-CH₄ (‰), and oxidation rates (nM d⁻¹; MOX – full lines, AOM – dashed lines) in the Gotland Sea sub-basin (cf. Fig. S1) year 2015. The upper panels illustrate monthly mean profiles from January to June; the lower panels illustrate monthly mean profiles from July to December.

Observations from 2012 indicate CH₄ concentrations in a range from ~1000 to 3000 nM in stagnant deep waters of the Baltic Proper (Jakobs et al., 2013), and values below ~150 nM in oxic deep waters in the same area after a major deep-water intrusion in winter 2014–2015 (Schmale et al., 2016; Myllykangas et al., 2017). These values are well reproduced by the model (Fig. 3)

using the settings listed in Table 1, which implies that the simulated sediment CH_4 source is likely close to the real source, at least in the deep water where AOM rates are apparently very low (<0.1 nM d^{-1}; Jakobs et al., 2014). The simulated benthic CH_4 release from the seafloor amounts to 50 µmol CH_4 m^{-2} d^{-1} in the standard model run (Table 1), corresponding to ~0.3 g
410 CH_4 m^{-2} y^{-1}. This is in the lower range of yearly observations at shallow coastal sites among varying habitats in the Baltic Sea (0.34-0.55 g CH_4 m^{-2} y^{-1}; Roth et al., 2023).

Measurements from the central Gotland Sea indicate typical surface water CH_4 concentrations in a range 3.5-5 nM, depending on the season (Gülzow et al., 2013), with the highest concentrations observed in winter because of increased gas solubility in cold water. This seasonal cycle is reproduced by the model (Fig. 3). Furthermore, simulated surface water CH_4 saturation
415 levels vary between approximately 110% in winter and 150% in summer (Fig. S5), which reproduces observed saturation levels (Gülzow et al., 2013).

Measurements from the central Baltic Sea indicate MOX rates ranging from 0.1 to 4 nM d^{-1} in the redox zone (Schmale et al., 2012; 2016; Jakobs et al., 2014). In the standard model run, the highest oxidation rates (> 3 nM d^{-1}; Fig. 5) occur in the deep water after deep water intrusions leading to oxygenation of stagnant water with high CH_4 concentrations. In the redox zone,
420 the simulated MOX rates are typically in a range 0.5-3 nM d^{-1} (Fig. 4-5), which thus matches observed oxidation rates. Simulated surface water MOX rates are in a range 0.3-0.5 nM d^{-1} (e.g., Fig. 3), whereas observations, on the other hand, indicate rates close to zero (Jakobs et al., 2014).

Observations indicate a pronounced ^{13}C-CH_4 enrichment in the redox zone. Based on two profiles from 2012, $\delta^{13}C$-CH_4 increased from values below -70‰ at the bottom of the redox zone (~140 m) to -40‰ at the top of the redox zone (~80 m) in
425 the central Gotland Sea (Jakobs et al., 2014). The $\delta^{13}C$-CH_4 peak values at intermediate depths coincide with peak oxidation rates (Jakobs et al., 2014) and result from the preferential oxidation of the lighter isotope. In water above the top of the redox zone, observations indicate lower oxidation rates and $\delta^{13}C$-CH_4 values in a range -60‰ to -40‰ depending on season (Jakobs et al., 2014). In the standard model run, the $\delta^{13}C$-CH_4 value typically increases from approximately -70‰ at the upper limit for anoxic water (~130 m) to its peak values between -45‰ and -40‰ at approximately 75 m (Fig. 4). The simulated $\delta^{13}C$-
430 CH_4 in the redox zone thus tends to be less pronounced than what is apparent from the few available observations. Furthermore, a local minimum around 30 m observed by Jakobs et al. (2014) is not reproduced in the model run.

3.2 Preliminary CH_4 budget

Here, we present preliminary budget calculations based on the standard model run. It is however important to stress that these estimates are heavily dependent on the prescribed benthic CH_4 source. As discussed below (Sect. 4), different combinations
435 of benthic CH_4 release and MOX rates could produce similar CH_4 concentrations in the water column.

Total CH_4 sources (land load and sediment release) and sinks (outgassing, net export, and pelagic oxidation) were aggregated over the entire Baltic Sea to allow a preliminary assessment of the relative importance of different processes. The CH_4 sources were largely dominated by benthic release which amounted to an average 7557 Mmol y^{-1} over the 2001-2020 period (Table 2). This source was mainly balanced by oxidation in the water column (6598 Mmol y^{-1}, 87% of the sinks) and to a smaller

440   degree by emission to the atmosphere (980 Mmol y^{-1}, 13% of the sinks). The land load (49 Mmol y^{-1}) and net export to the North Sea (19 Mmol y^{-1}) were comparatively small.

Table 2. Total CH$_4$ sources, sinks, and net change (= sources - sinks) (Mmol y^{-1}) aggregated over the entire Baltic Sea and averaged over the period 2001-2020.

CH$_4$ sources, sinks, and net change	CH$_4$ flux (Mmol y^{-1})
Land load	49
Air-sea exchange	-980
Net export	-19
Pelagic oxidation	-6598
Sediment release	7557
Net change	9

445

Figure 6 illustrates simulated monthly fluxes, net accumulation as well as the total amount of CH$_4$ in the entire Baltic Sea. The total CH$_4$ stock amounted to approximately 1800 Mmol y^{-1} over the ~2010-2014 period, which exceeded the stock before and after that period by a factor 2-3 (Fig. 6). This comparatively large CH$_4$ stock was the result of a large anoxic deep-water volume and thus low oxidation rates (Fig. 2). There was an average net accumulation of 9 Mmol y^{-1} over the 2001-2020 period (Table

450   2), but net changes of the total CH$_4$ stock between individual years varied by approximately ± 50 Mmol mo^{-1}, which largely reflected oxygen dependent changes in CH$_4$ oxidation rates (Fig. 6).
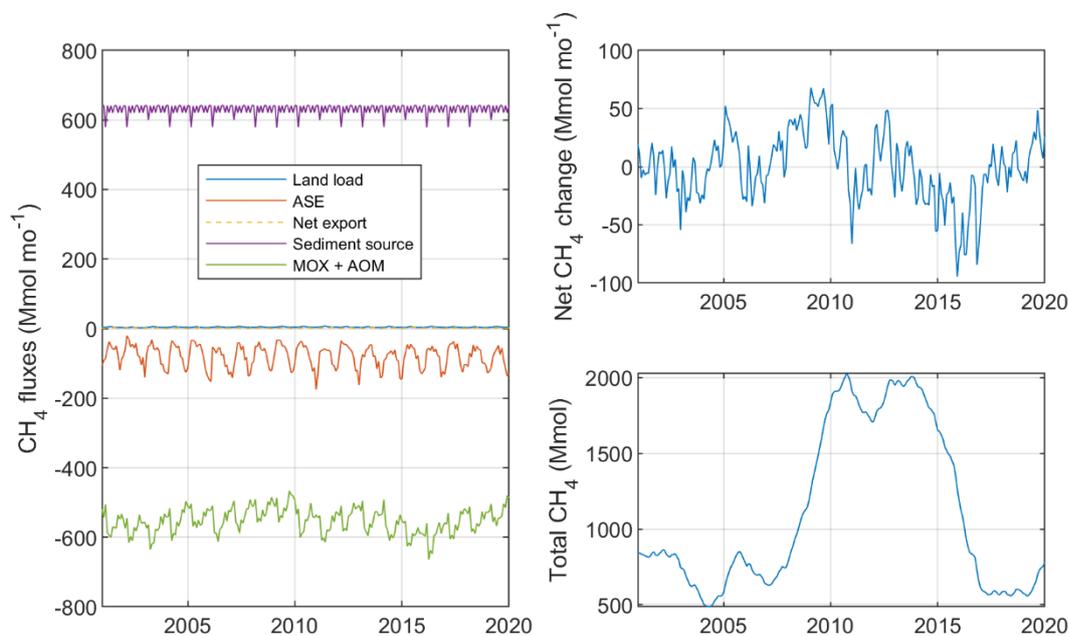
Figure 6: Simulated annual mean CH$_4$ sources and sinks (Mmol mo^{-1}; left), net change (= sources - sinks) (Mmol mo^{-1}; upper right), and total CH$_4$ stock (Mmol; lower right) aggregated over the entire Baltic Sea.

4 Discussion

This study presents a first quantification of key CH$_4$ fluxes on a Baltic Sea scale. However, there are uncertainties in our estimates, in particular regarding the benthic CH$_4$ source. In the standard model run, benthic release is the dominant CH$_4$ source (Table 2). The sediment source is set as constant over time, at all depths, and in all sub-basins. In the real Baltic Sea, however, large spatial and temporal variations are expected (e.g., Roth et al., 2022). Furthermore, the isotopic composition of the sediment source is set either to -80‰ or -60‰ depending on oxygen conditions in the overlying water. This assumption is a simplified representation. The main uncertainty in our present large-scale estimates is that spatial and temporal variations of the sediment source are not well known.

The simulated CH$_4$ concentrations in anoxic deep waters agree with available observations. The calibrated rate of CH$_4$ release from sediments is for that reason deemed as feasible in anoxic deep waters, since CH$_4$ concentrations are only marginally influenced by oxidation during anoxic conditions (low AOM rates).

It is more challenging to constrain the sediment source in shallower oxic waters, where the source can be largely compensated by MOX in the water column. Coastal systems are also more dynamic and show a larger variety compared to deep anoxic areas. A large CH$_4$ source compensated by high MOX rates could for example yield similar CH$_4$ concentrations as a smaller

source combined with lower MOX rates. These two different cases (i.e., large source, high oxidation vs. small source, low oxidation) would produce quite different isotopic patterns that could be used to calibrate the model. However, a complication here is that we generally do not know the isotopic composition of CH_4 released from the sediments, with the exception of observational data from a few locations. Justification of the calibrated rates used in the model would require more observational

475   data to fill the knowledge gaps.

The calibrated parameter values used in the computation of MOX rates (Eq. 16) differ substantially from other published estimates from lake studies (e.g., Greene et al., 2014; Tan et al., 2015; Bayer et al., 2019). Here, these parameters were calibrated so that the resulting profiles of oxidation rates and isotopic composition – as well as CH_4 concentrations – reasonably well reproduce observed profiles from the central Baltic Sea. Results for CH_4 concentrations, MOX rates, and isotopic

480   composition are sensitive to O_2 profiles, which also means that the calibrated values depend on how well the model reproduces O_2 concentrations.

The rate constant for MOX depends on the activity and abundance of methanotrophs, in theory allowing for reduced MOX in spite of favorable conditions in terms of CH_4 and O_2 concentrations when methanotrophs are not active. The model does not include methanotrophic activity explicitly, and the rate constant for MOX is constant. Perhaps, lower abundance and activity

485   of methanotrophs could be an explanation for the lower rate constant in the present results compared to the results from lakes cited above.

It is furthermore worth to mention here that Schmale et al. (2018) described an unresolved CH_4 source in oxic upper waters of the central Baltic Sea, possibly related to zooplankton activity. This source has not been addressed in the present study.

4.1 Sensitivity experiments

490   A series of sensitivity experiments was performed on different parameters used in the modeling of CH_4 and its stable isotopes (Table 1). The adjusted parameter values are listed in Table 3. Modeled profiles are then drawn for both winter conditions (February) and summer conditions (August) of 2015 (Fig. S6-S11), which gives an indication of season dependent contrasting conditions in surface waters above the halocline. Methane cycling in the model is largely dominated by benthic release, oxidation in the water column, and outgassing (Table 2; Fig. 6). For that reason, sensitivity experiments on riverine and North

495   Sea CH_4 concentrations were not included.

Table 3. Adjusted parameter values and change (%) compared to the standard model run in the various sensitivity experiments.

Model run	Adjusted parameter	Notation	Value	Unit
test 1	Potential maximum oxidation rate (MOX)	v_{WCH4_O2}	4 (-50%)	nM d^{-1}
test 2	Potential maximum oxidation rate (MOX)	v_{WCH4_O2}	12 (+50%)	nM d^{-1}
test 3	Half saturation value, CH_4 oxidation	h_{CH4}	30 (-50%)	nM
test 4	Half saturation value, CH_4 oxidation	h_{CH4}	90 (+50%)	nM

test 5	Half saturation value, CH$_4$ oxidation	h_{O2}	50 (-50%)	μM
test 6	Half saturation value, CH$_4$ oxidation	h_{O2}	150 (+50%)	μM
test 7	Fractionation, CH$_4$ oxidation	α_{oxi}	0.984 (-4‰)	-
test 8	Fractionation, CH$_4$ oxidation	α_{oxi}	0.992 (+4‰)	-
test 9	Sediment source, δ^{13}C-CH$_4$, oxic water	$\delta^{13}C\text{-}CH_{4sed}$	-70 (-10‰)	‰
test 10	Sediment source, δ^{13}C-CH$_4$, oxic water	$\delta^{13}C\text{-}CH_{4sed}$	-50 (+10‰)	‰
test 11	Sediment source, CH$_4$ flux, oxic water	r_{SED}	25 (-50%)	μmol m^{-2} d^{-1}
test 12	Sediment source, CH$_4$ flux, oxic water	r_{SED}	75 (+50%)	μmol m^{-2} d^{-1}

4.1.1 MOX and AOM: rates, half-saturation constants, and fractionation

500 Adjusting the potential maximum rate of MOX (v_{WCH4_O2}) by ± 50% (tests 1-2) has a large influence on CH$_4$ concentrations (Fig. S6), where decreased v_{WCH4_O2} (test 1) leads to substantially higher CH$_4$ concentrations, and increased v_{WCH4_O2} (test 2) to lower CH$_4$ compared to the standard model run. Since the MOX rate in addition to v_{WCH4_O2} depends on CH$_4$ concentration, the changed CH$_4$ concentration in itself will further modify the shape of the MOX profile (CH$_4$ oxidation also consumes O$_2$, but the influence on O$_2$ concentration is small compared to the influence on CH$_4$ concentration, since O$_2$ and CH$_4$ typically

505 differ by orders of magnitude). The modified shapes of the MOX profiles also influence the δ^{13}C-CH$_4$ profiles, with changed depths of the intermediate deep-water peak as well as changed peak values. Adjusting the potential maximum rate of AOM (v_{WCH4_SO4}) has a comparatively minor influence on both CH$_4$ concentration and isotopic composition because of the low anaerobic oxidation rates (not shown).

Adjusting the half saturation values for CH$_4$ oxidation (h_{CH4} and h_{O2}) by ± 50% (tests 3-6) influences the MOX rates and thus

510 both the CH$_4$ concentration and the isotopic composition (Fig. S7-S8). These parameters alter the dynamics within a relatively small range close to their respective values. Thus, the MOX rate is most sensitive to changes of h_{CH4} where the CH$_4$ concentration is close to 60 nM, and similarly, most sensitive to changes of h_{O2} where the O$_2$ concentration is close to 100 μM (Table 1). At high concentrations compared to the values of h_{CH4} and h_{O2}, we do not expect a large impact by adjusting these constants. On the other hand: at low concentrations compared to the constants, the sensitivity to changed values of h_{CH4} and

515 h_{O2} is expected to be similar to changing the potential maximum rate constant (v_{WCH4_O2}).

In these particular experiments, CH$_4$ dynamics are more sensitive to changes in h_{O2} than h_{CH4}, and the reason for this is the relatively large water volume where the O$_2$ concentration is close to h_{O2}, while the CH$_4$ concentration on the other hand is only close to h_{CH4} in a comparatively narrow band at intermediate depths. The modified CH$_4$ dynamics are, however, transferred to other depths by turbulent diffusion and vertical internal circulation ('old' water mixing into the intruding new deep water),

520 which means that altered CH$_4$ concentrations, δ values, and MOX rates are (more or less) apparent throughout the entire water column.

Adjusting the fractionation during CH_4 oxidation by $\pm$ 4‰ (tests 7-8) has no influence on CH_4 oxidation rates and concentrations, but a relatively strong (and predictable) impact on $\delta^{13}C$-CH_4 values throughout the entire water column (Fig. S9).

4.1.2 Sediment source: CH₄ release and isotopic composition

As indicated in Sect. 4, it is expected that the isotopic composition of the sediment source differs between different locations depending on the degree of oxidation in the pore water. The rate of CH_4 release is also expected to depend on the balance between benthic CH_4 production and oxidation, respectively. Adjusting the $\delta^{13}C$-CH_4 value of the sediment source by $\pm$ 10‰ during oxic conditions (tests 9-10) has no influence on CH_4 oxidation rates and concentrations, but a strong (and predictable) impact on $\delta^{13}C$-CH_4 profiles (Fig. S10).

In experiments where the rate of CH_4 release from the sediments source was adjusted by $\pm$ 50‰ during oxic conditions (tests 11-12), strong impacts are apparent for both the CH_4 concentration and isotopic composition throughout the water column. Deep water MOX rates are however less sensitive since the rates in these cases depend more on O_2 concentration – which is very similar between the two experiments (not shown) – than CH_4 concentrations (Fig. S11).

4.2 Caveats and outlook

As previously discussed, the main uncertainty in the model simulations lies in our limited understanding of CH_4 release from different sediment areas, as well as the isotopic composition of CH_4 released into the water column. Both the flux and the isotopic composition depend on the balance between production and oxidation rates in the sediment. A high production could be compensated by high oxidation and thus result in a relatively small CH_4 release to the water column in spite of a large production. This would then be evident by a ^{13}C-CH_4 enrichment, i.e., comparatively heavy CH_4. Alternatively, a relatively small CH_4 production could still result in a substantial release to the water column in a case where the oxidation rate is low, which would then also be evident by CH_4 depleted in ^{13}C-CH_4, i.e., comparatively light CH_4.

Improved knowledge of properties of CH_4 released from sediment to water column in different areas of the Baltic Sea (e.g., the Kattegat and the major gulfs – the Gulf of Bothnia, Gulf of Riga, and Gulf of Finland) would help to improve model parameterizations and thus reduce the main uncertainties of model simulations. This was, however, beyond the scope of the present study because of the missing knowledge concerning both temporal and spatial patterns of the CH_4 source. A logical progression at this stage would involve detailed observations combined with modeling studies focused on processes in the sediments, i.e., production and oxidation rates, depending on carbon accumulation rate, oxygen conditions, and the presence of methanotrophs.

A crucial missing link in this study is the formation, transport, and fate of CH_4 bubbles. Ebullition has been included in lake models (e.g., Greene et al., 2014; Bayer et al., 2019); however, we do not have experimental data to calibrate and validate the large-scale influence of ebullition in the Baltic Sea. The calibrated benthic CH_4 source represents a "bulk" CH_4 release, including in theory both the influences of diffusive flux and bubble dissolution on CH_4 concentrations in the water column.

555   However, CH$_4$ ebullition might bypass methanotrophy and consequently contribute to higher CH$_4$ emissions, in particular in shallow-water areas (Broman et al., 2020). This indicates that the simulated CH$_4$ outgassing is likely underestimating the real outgassing from the Baltic Sea. Observations of ebullitive fluxes in combination with development of model parameterizations represent important steps to better describe and quantify CH$_4$ emissions from the Baltic Sea.

  Roth et al. (2023) observed significant CH$_4$ production and release from vegetated oxic shallow-water areas. BALTSEM-CH$_4$ v1.0 does not differentiate between vegetated and unvegetated areas, which means that this CH$_4$ source – and its contribution

560   to outgassing – could not be addressed here, which consequently represents another gap in our current understanding. Both species distribution models and process-based models for vegetation exist (e.g., Lappalainen et al., 2019; Graiff et al., 2020), but to our knowledge do not include CH$_4$ dynamics. Hence, the inclusion of CH$_4$ in vegetation models could potentially serve as an objective for future scientific projects.

  The process parameterizations used in this study to describe large-scale CH$_4$ cycling in the Baltic Sea can also be applied in

565   various other domains. As part of our future plans, we aim to investigate CH$_4$ dynamics in a smaller area where more observations are available and where the CH$_4$ concentration and isotopic composition, as well as properties of end-members (river load, benthic release, and lateral boundary conditions), are better understood. This would further help to constrain process rates in the model.

  The calculated average total CH$_4$ emission of 980 Mmol y^{-1} corresponds to approximately 0.04 g CH$_4$ m^{-2} y^{-1}, and constitutes

570   only about 13% of the calibrated sediment source (~0.3 g CH$_4$ m^{-2} y^{-1}). The model includes both shallow- and deep water sediment areas, but the calibrated sediment source is in the lower range of rates reported for a shallow-water coastal area (0.34-0.55 g CH$_4$ m^{-2} y^{-1}; Roth et al., 2023), indicating that the model might not well represent coastal CH$_4$ hotspots. One major knowledge gap at this point is the relative importance of shallow coastal areas compared to the open Baltic Sea in terms of CH$_4$ outgassing. This is an important scientific question that needs to be addressed in future studies.

575   **Code and data availability**

  All model output data for the standard model run, as well as the version of the model source code used in this study are archived on Zenodo at https://doi.org/10.5281/zenodo.10037197 (last access: 24 October 2023). In addition to model output and source code, the archive includes initial profiles, boundary conditions, meteorological forcing, runoff, as well as land loads and atmospheric depositions of dissolved and particulate constituents.

580   **Author contributions**

  E.G. wrote the first draft of the manuscript with contributions from all co-authors. E.G. developed the CH$_4$ model components, and designed and performed the model experiments and analyses. B.G. is the main developer of the BALTSEM model.

Competing interests

585   The contact author has declared that none of the authors has any competing interests.

Acknowledgements

This research is part of the University of Helsinki and Stockholm University collaborative research initiative (CoastClim, www.coastclim.org; The Baltic Bridge initiative). The Baltic Nest Institute is supported by The Swedish Agency for Marine and Water Management through their grant 1:11 – Measures for marine and water environment.

590   **Appendix A: State variables and biogeochemical transformation processes**

Table A1. Pelagic and sediment state variables in BALTSEM-CH$_4$ v1.0.

State variable	Description	Unit
Pelagic		
SAL	Salinity	-
T	Temperature	°C
OXY	Dissolved oxygen	g O$_2$ m^{-3}
NH	Reduced N (NH$_4^+$ + NH$_3$)	mg N m^{-3}
NO	Oxidized N (NO$_3^-$ + NO$_2^-$)	mg N m^{-3}
PO	Dissolved inorganic phosphorus (H$_3$PO$_4$ + H$_2$PO$_4^-$ + HPO$_4^=$ + PO$_4^{3-}$)	mg P m^{-3}
SiO	Silicate (Si(OH)$_4$ + SiO(OH)$_3^-$)	mg Si m^{-3}
DETN	Detrital N	mg N m^{-3}
DETP	Detrital P	mg P m^{-3}
DETSi	Detrital Si, biogenic Si	mg Si m^{-3}
DETCm	Detrital C (autochthonous)	mg C m^{-3}
DETCt	Detrital C (allochthonous)	mg C m^{-3}
PHY1	Phytoplankton group 1, N$_2$ fixers	mg N m^{-3}
PHY2	Phytoplankton group 2, diatoms	mg N m^{-3}
PHY3	Phytoplankton group 3, other phytoplankton	mg N m^{-3}
ZOO	Zooplankton community	mg N m^{-3}
DONL	Labile dissolved organic N	mg N m^{-3}
DONR	Refractory dissolved organic N	mg N m^{-3}
DOPL	Labile dissolved organic P	mg P m^{-3}

DOPR	Refractory dissolved organic P	mg P m^{-3}
DOCLt	Labile dissolved organic C (allochthonous)	mg C m^{-3}
DOCRt	Refractory dissolved organic C (allochthonous)	mg C m^{-3}
DOCLm	Labile dissolved organic C (autochthonous)	mg C m^{-3}
DOCRm	Refractory dissolved organic C (autochthonous)	mg C m^{-3}
DIC	Dissolved inorganic carbon ($CO_2 + H_2CO_3 + HCO_3^- + CO_3^{2-}$)	mmol m^{-3}
ALK	Total alkalinity	mmol m^{-3}
HS	Total hydrogen sulfide ($HS^- + H_2S$)	mg S m^{-3}
12CH4	^{12}C methane	µmol m^{-3}
13CH4	^{13}C methane	µmol m^{-3}
Sediment		
SEDN	Sedimentary organic N	mg N m^{-2}
SEDP	Sedimentary organic P	mg P m^{-2}
SEDSi	Sedimentary biogenic Si	mg Si m^{-2}
SEDCm	Sedimentary organic C (autochthonous)	mg C m^{-2}
SEDCt	Sedimentary organic C (allochthonous)	mg C m^{-2}

Appendix B: Model forcing

Model forcing consists of actual weather data and observed nutrient loads as well as calibrated carbon and total alkalinity loads (Gustafsson and Gustafsson, 2020) covering the period 1970-2020. River runoff, land loads, and atmospheric depositions were

595 based on Pollution Load Compilation data (PLC; HELCOM, 2021) as well as other sources (Gustafsson et al., 2012). Atmospheric forcing was constructed from data provided by the Swedish Meteorological and Hydrological Institute (SMHI): RCA-ERA40 (1970-2006), Hirlam-Mesan (2007-2015), and Arome-Mesan (2016-2020). The Kattegat water level and also boundary conditions in the Skagerrak were based on data provided by the SMHI (Gustafsson et al., 2012).

References

600 Atkins, M. L., Santos, I. R., and Maher, D. T.: Seasonal exports and drivers of dissolved inorganic and organic carbon, carbon dioxide, methane and δ^{13}C signatures in a subtropical river network, Science of The Total Environment, 575, 545–563, https://doi.org/10.1016/j.scitotenv.2016.09.020, 2017.

Bange, H. W., Bartell, U. H., Rapsomanikis, S., and Andreae, M. O.: Methane in the Baltic and North Seas and a reassessment of the marine emissions of methane, Global Biogeochem. Cycles, 8, 465–480, https://doi.org/10.1029/94GB02181, 1994.

605   Borges, A. V., Champenois, W., Gypens, N., Delille, B., and Harlay, J.: Massive marine methane emissions from near-shore shallow coastal areas, Sci Rep, 6, 27908, https://doi.org/10.1038/srep27908, 2016.

Broman, E., Sun, X., Stranne, C., Salgado, M. G., Bonaglia, S., Geibel, M., Jakobsson, M., Norkko, A., Humborg, C., and Nascimento, F. J. A.: Low Abundance of Methanotrophs in Sediments of Shallow Boreal Coastal Zones With High Water Methane Concentrations, Frontiers in Microbiology, 11, https://doi.org/10.3389/fmicb.2020.01536, 2020.

610   Chuang, P.-C., Yang, T. F., Wallmann, K., Matsumoto, R., Hu, C.-Y., Chen, H.-W., Lin, S., Sun, C.-H., Li, H.-C., Wang, Y., and Dale, A. W.: Carbon isotope exchange during anaerobic oxidation of methane (AOM) in sediments of the northeastern South China Sea, Geochimica et Cosmochimica Acta, 246, 138–155, https://doi.org/10.1016/j.gca.2018.11.003, 2019.

Dickson, A. G., Sabine, C. L., and Christian, J. R. (Eds.): Guide to best practices for ocean CO_2 measurements. PICES Special Publication 3, North Pacific Marine Science Organization, Sidney, BC, 191 pp., 2007.

615   Egger, M., Hagens, M., Sapart, C. J., Dijkstra, N., van Helmond, N. A. G. M., Mogollón, J. M., Risgaard-Petersen, N., van der Veen, C., Kasten, S., Riedinger, N., Böttcher, M. E., Röckmann, T., Jørgensen, B. B., and Slomp, C. P.: Iron oxide reduction in methane-rich deep Baltic Sea sediments, Geochimica et Cosmochimica Acta, 207, 256–276, https://doi.org/10.1016/j.gca.2017.03.019, 2017.

Fuex, A. N.: Experimental evidence against an appreciable isotopic fractionation of methane during migration, Physics and
620   Chemistry of the Earth, 12, 725–732, https://doi.org/10.1016/0079-1946(79)90153-8, 1980.

Graiff, A., Karsten, U., Radtke, H., Wahl, M., and Eggert, A.: Model simulation of seasonal growth of Fucus vesiculosus in its benthic community, Limnology and Oceanography: Methods, 18, 89–115, https://doi.org/10.1002/lom3.10351, 2020.

Grunwald, M., Dellwig, O., Beck, M., Dippner, J. W., Freund, J. A., Kohlmeier, C., Schnetger, B., and Brumsack, H.-J.: Methane in the southern North Sea: Sources, spatial distribution and budgets, Estuarine, Coastal and Shelf Science, 81, 445–
625   456, https://doi.org/10.1016/j.ecss.2008.11.021, 2009.

Gu, C., Waldron, S., and Bass, A. M.: Carbon dioxide, methane, and dissolved carbon dynamics in an urbanized river system, Hydrological Processes, 35, e14360, https://doi.org/10.1002/hyp.14360, 2021.

Gustafsson, E. and Gustafsson, B. G.: Future acidification of the Baltic Sea – A sensitivity study, Journal of Marine Systems, 211, 103397, https://doi.org/10.1016/j.jmarsys.2020.103397, 2020.

630   Gustafsson, E., Carstensen, J., Fleming, V., Gustafsson, B. G., Hoikkala, L., and Rehder, G.: Causes and consequences of acidification in the Baltic Sea: implications for monitoring and management, Sci Rep, 13, 16322, https://doi.org/10.1038/s41598-023-43596-8, 2023.

Gustafsson, E., Savchuk, O. P., Gustafsson, B. G., and Müller-Karulis, B.: Key processes in the coupled carbon, nitrogen, and phosphorus cycling of the Baltic Sea, Biogeochemistry, 134, 301–317, https://doi.org/10.1007/s10533-017-0361-6, 2017.

635   Gustafsson, B. G., Schenk, F., Blenckner, T., Eilola, K., Meier, H. E. M., Müller-Karulis, B., Neumann, T., Ruoho-Airola, T., Savchuk, O. P., and Zorita, E.: Reconstructing the Development of Baltic Sea Eutrophication 1850–2006, AMBIO, 41, 534–548, https://doi.org/10.1007/s13280-012-0318-x, 2012.

Gülzow, W., Gräwe, U., Kedzior, S., Schmale, O., and Rehder, G.: Seasonal variation of methane in the water column of Arkona and Bornholm Basin, western Baltic Sea, Journal of Marine Systems, 139, 332–347, https://doi.org/10.1016/j.jmarsys.2014.07.013, 2014.

Gülzow, W., Rehder, G., Schneider v. Deimling, J., Seifert, T., and Tóth, Z.: One year of continuous measurements constraining methane emissions from the Baltic Sea to the atmosphere using a ship of opportunity, Biogeosciences, 10, 81–99, https://doi.org/10.5194/bg-10-81-2013, 2013.

Happell, J. D., Chanton, J. P., and Showers, W. J.: Methane transfer across the water-air interface in stagnant wooded swamps of Florida: Evaluation of mass-transfer coefficients and isotropic fractionation, Limnology and Oceanography, 40, 290–298, https://doi.org/10.4319/lo.1995.40.2.0290, 1995.

HELCOM: HELCOM Baltic Sea Action Plan – 2021 update. Available at http://helcom.fi, 2021.

Hoehler, T. M., Alperin, M. J., Albert, D. B., and Martens, C. S.: Field and laboratory studies of methane oxidation in an anoxic marine sediment: Evidence for a methanogen-sulfate reducer consortium, Global Biogeochemical Cycles, 8, 451–463, https://doi.org/10.1029/94GB01800, 1994.

Hoffman, D. W. and Rasmussen, C.: Absolute Carbon Stable Isotope Ratio in the Vienna Peedee Belemnite Isotope Reference Determined by 1H NMR Spectroscopy, Anal. Chem., 94, 5240–5247, https://doi.org/10.1021/acs.analchem.1c04565, 2022.

Holmes, M. E., Sansone, F. J., Rust, T. M., and Popp, B. N.: Methane production, consumption, and air-sea exchange in the open ocean: An Evaluation based on carbon isotopic ratios, Global Biogeochemical Cycles, 14, 1–10, https://doi.org/10.1029/1999GB001209, 2000.

Humborg, C., Geibel, Marc. C., Sun, X., McCrackin, M., Mörth, C.-M., Stranne, C., Jakobsson, M., Gustafsson, B., Sokolov, A., Norkko, A., and Norkko, J.: High Emissions of Carbon Dioxide and Methane From the Coastal Baltic Sea at the End of a Summer Heat Wave, Frontiers in Marine Science, 6, https://doi.org/10.3389/fmars.2019.00493, 2019.

Jakobs, G., Holtermann, P., Berndmeyer, C., Rehder, G., Blumenberg, M., Jost, G., Nausch, G., and Schmale, O.: Seasonal and spatial methane dynamics in the water column of the central Baltic Sea (Gotland Sea), Continental Shelf Research, 91, 12–25, https://doi.org/10.1016/j.csr.2014.07.005, 2014.

Jakobs, G., Rehder, G., Jost, G., Kießlich, K., Labrenz, M., and Schmale, O.: Comparative studies of pelagic microbial methane oxidation within the redox zones of the Gotland Deep and Landsort Deep (central Baltic Sea), Biogeosciences, 10, 7863–7875, https://doi.org/10.5194/bg-10-7863-2013, 2013.

Jørgensen, B. B., Bang, M., and Blackburn, T.: Anaerobic mineralization in marine sediments from the Baltic Sea-North Sea transition, Marine Ecology Progress Series, 59, 39–54, 1990.

Knox, M., Quay, P. D., and Wilbur, D.: Kinetic isotopic fractionation during air-water gas transfer of O_2, N_2, CH_4, and H_2, Journal of Geophysical Research: Oceans, 97, 20335–20343, https://doi.org/10.1029/92JC00949, 1992.

Kremling, K.: Untersuchungen Über die chemische Zusammensetzung des Meerwassers aus der Ostsee, III. Früjahr 1969-Herbst 1970, Kiel. Meeresforsch., 28, 99-118. https://oceanrep.geomar.de/id/eprint/54305/, 1972.

Kuliński, K., Rehder, G., Asmala, E., Bartosova, A., Carstensen, J., Gustafsson, B., Hall, P. O. J., Humborg, C., Jilbert, T., Jürgens, K., Meier, H. E. M., Müller-Karulis, B., Naumann, M., Olesen, J. E., Savchuk, O., Schramm, A., Slomp, C. P., Sofiev, M., Sobek, A., Szymczycha, B., and Undeman, E.: Biogeochemical functioning of the Baltic Sea, Earth System Dynamics, 13, 633–685, https://doi.org/10.5194/esd-13-633-2022, 2022.

675 Lan, X., Basu, S., Schwietzke, S., Bruhwiler, L. M. P., Dlugokencky, E. J., Michel, S. E., Sherwood, O. A., Tans, P. P., Thoning, K., Etiope, G., Zhuang, Q., Liu, L., Oh, Y., Miller, J. B., Pétron, G., Vaughn, B. H., and Crippa, M.: Improved Constraints on Global Methane Emissions and Sinks Using δ^{13}C-CH$_4$, Global Biogeochemical Cycles, 35, e2021GB007000, https://doi.org/10.1029/2021GB007000, 2021.

Lappalainen, J., Virtanen, E. A., Kallio, K., Junttila, S., and Viitasalo, M.: Substrate limitation of a habitat-forming genus
680 Fucus under different water clarity scenarios in the northern Baltic Sea, Estuarine, Coastal and Shelf Science, 218, 31–38, https://doi.org/10.1016/j.ecss.2018.11.010, 2019.

Lundevall-Zara, M., Lundevall-Zara, E., and Brüchert, V.: Sea-Air Exchange of Methane in Shallow Inshore Areas of the Baltic Sea, Frontiers in Marine Science, 8, https://doi.org/10.3389/fmars.2021.657459, 2021.

Myllykangas, J.-P., Jilbert, T., Jakobs, G., Rehder, G., Werner, J., and Hietanen, S.: Effects of the 2014 major Baltic inflow
685 on methane and nitrous oxide dynamics in the water column of the central Baltic Sea, Earth System Dynamics, 8, 817–826, https://doi.org/10.5194/esd-8-817-2017, 2017.

Myllykangas, J.-P., Rissanen, A. J., Hietanen, S., and Jilbert, T.: Influence of electron acceptor availability and microbial community structure on sedimentary methane oxidation in a boreal estuary, Biogeochemistry, 148, 291–309, https://doi.org/10.1007/s10533-020-00660-z, 2020.

690 Osudar, R., Matoušů, A., Alawi, M., Wagner, D., and Bussmann, I.: Environmental factors affecting methane distribution and bacterial methane oxidation in the German Bight (North Sea), Estuarine, Coastal and Shelf Science, 160, 10–21, https://doi.org/10.1016/j.ecss.2015.03.028, 2015.

Quay, P. D., King, S. L., Lansdown, J. M., and Wilbur, D. O.: Isotopic composition of methane released from wetlands: Implications for the increase in atmospheric methane, Global Biogeochemical Cycles, 2, 385–397,
695 https://doi.org/10.1029/GB002i004p00385, 1988.

Reeburgh, W. S.: Oceanic Methane Biogeochemistry, Chem. Rev., 107, 486–513, https://doi.org/10.1021/cr050362v, 2007.

Rehder, G., Keir, R. S., Suess, E., and Pohlmann, T.: The Multiple Sources and Patterns of Methane inNorth Sea Waters, Aquatic Geochemistry, 4, 403–427, https://doi.org/10.1023/A:1009644600833, 1998.

Savchuk, O.P., Gustafsson, B.G., Müller-Karulis, B.: BALTSEM - a marine model for the decision support within the Baltic
700 Sea Region (Technical Report No. 7), BNI Technical Report Series, 2012.

Schmale, O., Blumenberg, M., Kießlich, K., Jakobs, G., Berndmeyer, C., Labrenz, M., Thiel, V., and Rehder, G.: Aerobic methanotrophy within the pelagic redox-zone of the Gotland Deep (central Baltic Sea), Biogeosciences, 9, 4969–4977, https://doi.org/10.5194/bg-9-4969-2012, 2012.

Schmale, O., Krause, S., Holtermann, P., Power Guerra, N. C., and Umlauf, L.: Dense bottom gravity currents and their impact

705   on pelagic methanotrophy at oxic/anoxic transition zones, Geophysical Research Letters, 43, 5225–5232, https://doi.org/10.1002/2016GL069032, 2016.

Schmale, O., Schneider von Deimling, J., Gülzow, W., Nausch, G., Waniek, J. J., and Rehder, G.: Distribution of methane in the water column of the Baltic Sea, Geophysical Research Letters, 37, https://doi.org/10.1029/2010GL043115, 2010.

Schmale, O., Wäge, J., Mohrholz, V., Wasmund, N., Gräwe, U., Rehder, G., Labrenz, M., and Loick-Wilde, N.: The

710   contribution of zooplankton to methane supersaturation in the oxygenated upper waters of the central Baltic Sea, Limnology and Oceanography, 63, 412–430, https://doi.org/10.1002/lno.10640, 2018.

Scranton, M. I. and McShane, K.: Methane fluxes in the southern North Sea: the role of European rivers, Continental Shelf Research, 11, 37–52, https://doi.org/10.1016/0278-4343(91)90033-3, 1991.

Slomp, C. P., Mort, H. P., Jilbert, T., Reed, D. C., Gustafsson, B. G., and Wolthers, M.: Coupled Dynamics of Iron and

715   Phosphorus in Sediments of an Oligotrophic Coastal Basin and the Impact of Anaerobic Oxidation of Methane, PLOS ONE, 8, e62386, https://doi.org/10.1371/journal.pone.0062386, 2013.

Upstill-Goddard, R. C., Barnes, J., Frost, T., Punshon, S., and Owens, N. J. P.: Methane in the southern North Sea: Low-salinity inputs, estuarine removal, and atmospheric flux, Global Biogeochemical Cycles, 14, 1205–1217, https://doi.org/10.1029/1999GB001236, 2000.

720   Van Bodegom, P., Goudriaan, J., and Leffelaar, P.: A mechanistic model on methane oxidation in a rice rhizosphere, Biogeochemistry, 55, 145–177, https://doi.org/10.1023/A:1010640515283, 2001.

Wallin, M. B., Campeau, A., Audet, J., Bastviken, D., Bishop, K., Kokic, J., Laudon, H., Lundin, E., Löfgren, S., Natchimuthu, S., Sobek, S., Teutschbein, C., Weyhenmeyer, G. A., and Grabs, T.: Carbon dioxide and methane emissions of Swedish low-order streams—a national estimate and lessons learnt from more than a decade of observations, Limnology and Oceanography

725   Letters, 3, 156–167, https://doi.org/10.1002/lol2.10061, 2018.

Wanninkhof, R.: Relationship between wind speed and gas exchange over the ocean revisited, Limnology and Oceanography: Methods, 12, 351–362, https://doi.org/10.4319/lom.2014.12.351, 2014.

Whiticar, M. J., Faber, E., and Schoell, M.: Biogenic methane formation in marine and freshwater environments: CO_2 reduction vs. acetate fermentation—Isotope evidence, Geochimica et Cosmochimica Acta, 50, 693–709, https://doi.org/10.1016/0016-

730   7037(86)90346-7, 1986.

Whiticar, M. J.: Carbon and hydrogen isotope systematics of bacterial formation and oxidation of methane, Chemical Geology, 161, 291–314, https://doi.org/10.1016/S0009-2541(99)00092-3, 1999.

Wiesenburg, D. A. and Guinasso, N. L.: Equilibrium solubilities of methane, carbon monoxide, and hydrogen in water and sea water, J. Chem. Eng. Data, 24, 356–360, https://doi.org/10.1021/je60083a006, 1979.

735   Wåhlström, I. and Meier, H. E. M.: A model sensitivity study for the sea–air exchange of methane in the Laptev Sea, Arctic Ocean, Tellus B, 66, https://doi.org/10.3402/tellusb.v66.24174, 2014.

Zeebe, R.E., Wolf-Gladrow, D.: CO_2 in seawater: equilibrium, kinetics, isotopes. Elsevier Oceanography Series. Amsterdam, Elsevier Science, B.V. 346 pp, 2001.